Digital image correlation data from analogue modelling experiments addressing orthogonal and rotational extension at the Tectonic Modelling Lab of the University of Bern (CH) (http://doi.org/10.5880/FIDGEO.2020.001)

Frank Zwaan[1], Guido Schreurs[2], Timothy Schmid[1], Michael Warsitzka[3], Matthias Rosenau[3,*]

1. Dipartimento di Scienze della Terra, Università di Studi di Firenze, Florence, Italy
2. Institute of Geological Sciences, University of Bern, Switzerland
3. GFZ German Research Centre for Geosciences, Potsdam, Germany

** Corresponding author: rosen@gfz-potsdam.de*

License

Creative Commons Attribution 4.0 International License (CC BY 4.0)

Citation

When using the data please cite:

Zwaan, Frank; Schreurs, Guido; Schmid, Timothy; Warsitzka, Michael; Rosenau, Matthias (2020): Digital image correlation data from analogue modelling experiments addressing orthogonal and rotational extension at the Tectonic Modelling Lab of the University of Bern (CH). GFZ Data Services. http://doi.org/10.5880/FIDGEO.2020.001

The data are supplementary material to:

Zwaan, Frank; Schreurs, Guido; Rosenau, Matthias (2019): Rift propagation in rotational versus orthogonal extension: Insights from 4D analogue models. Journal of Structural Geology. https://doi.org/10.1016/j.jsg.2019.103946

1. Data Description

This data set includes the results of digital image correlation of ten brittle-viscous experiments on crustal extension and four benchmarks performed at the Tectonic Modelling Lab of the University of Bern (UB). The experiments demonstrate the differences in rift development in orthogonal versus rotation extension. Detailed descriptions of the experiments and monitoring techniques can be found in Zwaan et al. (2019) to which this data set is supplementary. Additional background information concerning the general modelling approach are available in Zwaan et al. (2016). The data presented here consist of movies displaying the analogue model surface with the lateral displacement field and profiles of the lateral cumulative displacements.

1.1. Monitoring of experiments

All experiments (Table 1) were monitored with top view photographs (SLR camera Nikon D-100 6.1 Megapixel) taken every two minutes during the 4- or 5-hour model runs. Exceptions are experiments EXP661 and EXP666 which were photographed at one minute intervals and which were also monitored using a 64-slice Siemens Somatom Definition AS X-ray Computed Tomography (CT) scanner at 30 min time steps (i.e., a scan for every 4 mm of extension). CT-data was analyzed with the software OsiriX (Pixmeo SARL).

Table 1: Overview of experiments and benchmarks. *The lab code of the Tectonic Modelling Lab of the University of Bern (UB) is used throughout this data publication. 1 L = full length of model*

Experiment name in Zwaan et al. (2019)	Lab code UB	CT-scanned	Seed length	Extension velocity (mm/h)	Run time (hh:mm)	Image interval (min)	DIC interval (frame)
-	EXP771G (Benchmark)		-	10	04:00	2	25
-	EXP772 (Benchmark)		-	8	05:00	1	30
O1	EXP678		0	8	05:00	2	15
-	EXP681		¼ L	8	05:00	2	15
-	EXP680		½ L	8	05:00	2	15
-	EXP683		¾ L	8	05:00	2	15
O2*	EXP657		1 L	8	05:00	2	-
O3	EXP661	x	1 L	8	05:00	1 (CT: 30)	30
-	EXP771H (Benchmark)		-	8	05:00	1	30
-	EXP773 (Benchmark)		-	8	05:00	1	30
-	EXP679		0	8	05:00	2	15
-	EXP682		¼ L	8	05:00	2	15
-	EXP684		½ L	8	05:00	2	15
-	EXP685		¾ L	8	05:00	2	15
R2*	EXP658		1 L	8	05:00	2	-
R3	EXP666	x	1 L	8	05:00	1 (CT: 30)	30

* No DIC analysis available

1.2. Analysis method

1.2.1. Digital image correlation

Digital photographs of the experimental surface and digital image cross sections of the computed CT-scans were analyzed with digital image correlation (DIC; Adam et al., 2005, 2013) techniques to quantify horizontal displacements in the image plane at high precision (< 0.1 mm). DIC was undertaken with the software DaVis 8.0 (LaVision) applying 2D-DIC (FFT-legacy) multipass processing with a final interrogation window size of 32x32 (CT: 12x12) pixels and 50% (CT: 25%) overlap. The images were scaled, but not rectified. We verified the effect of rectification to be insignificant. DIC intervals were chosen such that the incremental extension is 4 mm in all experiments and benchmarks (Table 1) and calculated the cumulative displacement by means of adding the

increments in a Lagrangian reference frame. Results of the DIC are presented as movies showing the "across-strike displacement" (y-displacement) (Figure 1), i.e. displacement perpendicular to the strike of the experimental rift zone and parallel to the y-axis (= short axis of each image).

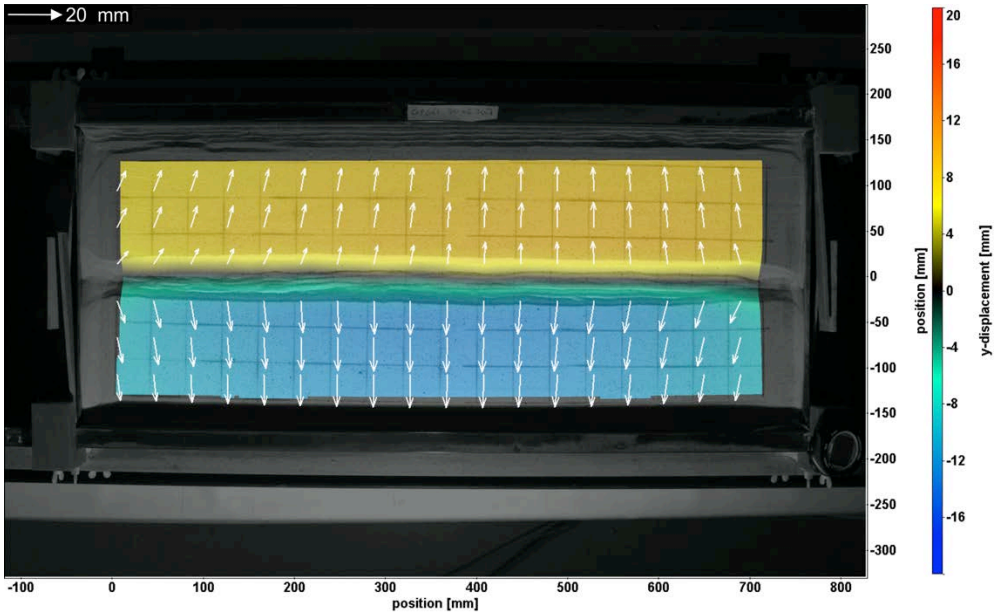

Figure 1: Example of DIC surface displacement results (EXP661). *Color-coded map and vectors of cumulative across-strike (y-) displacement. Exaggeration of vectors according to reference vector top left. See movies included in this data set.*

1.2.2. Profiles of cumulative surface displacement

The DIC-derived cumulative surface displacement vector field was further analyzed by extracting values of across-strike (y-)displacements along specified profiles aligned either parallel to the x-axis ("along-strike") or parallel to the y-axis ("across-strike"). The y and x positions of the along- and across-strike profiles are indicated in the file name. For each experiment, a Matlab-based script ("plotdata.m") is provided to automatically visualize y-displacement along the specified profile for each time step in one diagram (Figure 2). For Benchmark EXP773 a profile showing the along-strike (x-)displacement is provided.

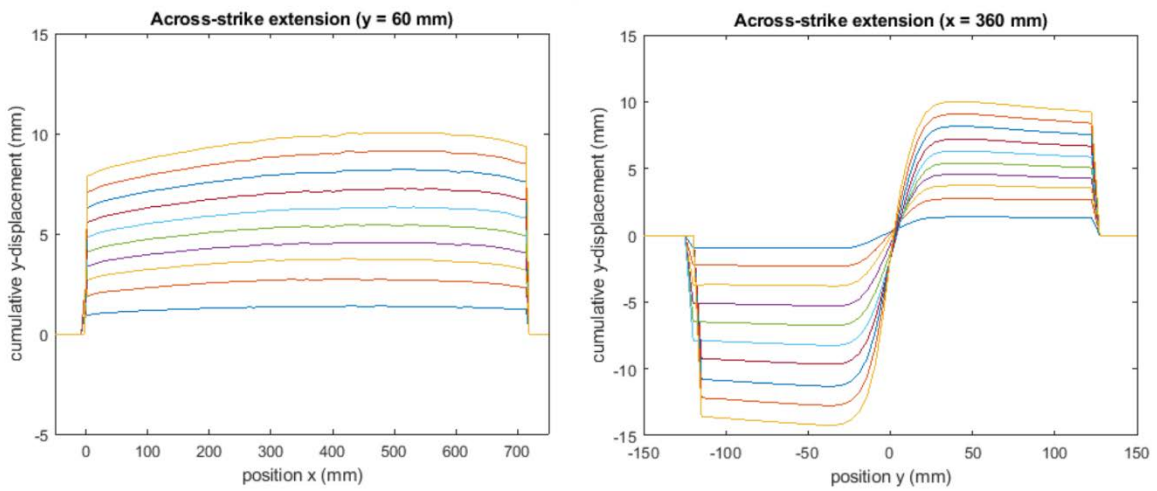

Figure 2: Example of a profile plot (EXP661). *Left: Cumulative across-strike y-displacements along an along-strike profile at a y-position of 60 mm. Right: Cumulative y-displacements along an across-strike profile at an x-position of 360 mm. Both diagrams show data for 10 successive time steps of 30 min each.*

1.2.3. Digital image correlation analysis of internal displacement

We also apply DIC on specific CT sections from EXP661 and EXP666. For both experiments we analyze along-strike sections through the center of the model, revealing along-strike displacement of model materials (Fig. 3). For EXP661 we present one section depicting the evolution of across-strike displacement in an extensional setting, whereas for EXP666 we also show results from its contractional domain. The locations of the along- and across-strike profiles are indicated in the list of files. Note that these DIC analyses on 2D CT data do not fully capture the complete 3D displacement field. Nevertheless, they provide a good indication of internal model deformation.

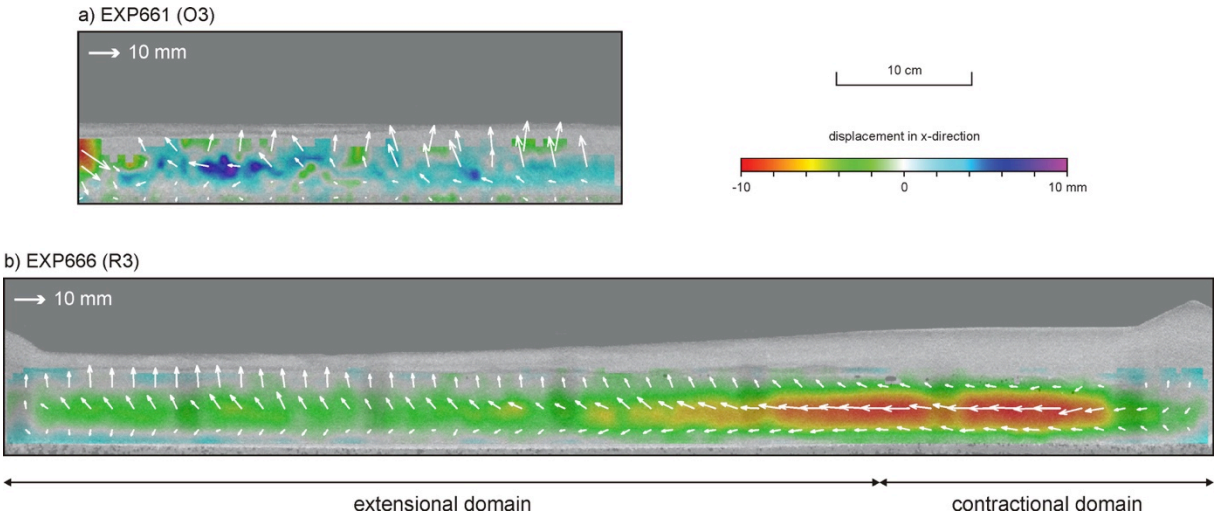

Figure 3: Example of DIC analysis on CT data from EXP661 and EXP666. *Cumulative along-strike x-displacements within a CT section along the axis of the experiment, showing (a) no clear flow patterns in orthogonal extension, or (b) clear viscous flow from the contractional domain (right) to the extensional domain (left). Exaggeration of vectors according to reference vector top left. See movies included in this data set.*

2. Experimental result description

2.1.1. Benchmark experiments

The experiments presented in Zwaan et al. (2019) contain important boundary effects (e.g. strain partitioning between rifts and model boundaries). In order to determine whether these are caused by the model base, test runs with only a foam layer were performed for both the orthogonal and rotational extension set-ups (EXP771G and EXP771H, respectively), and monitored by means of top view photography allowing for surface DIC analysis. These tests reveal that the foam deforms mostly homogeneously in both cases (Fig. 4), with either rift-perpendicular displacement (Fig. 4a) or rotational displacement (Fig. 4b). Note that EXP771G does show some rift-parallel shortening at its short ends (Fig. 4a). Additional trials with only a viscous layer on top of the foam base provide a similar result in orthogonal extension (EPX722) although the displacement pattern is more homogeneous (Fig. 4a, c). This suggests that any boundary effects seen on the model surface are associated with the presence of a brittle cover. The rotational experiment (EXP773) deviates from its orthogonal equivalent, as it develops a strong flow of viscous material from the contractional to the extensional domain (Fig. 4b, d). This is clearly due to variations in gravitational load, and is very similar to the lateral flow observed in EXP666 (Fig. 3), although viscous flow in the latter experiment is more restricted by the overlying brittle cover that does not deform as readily.

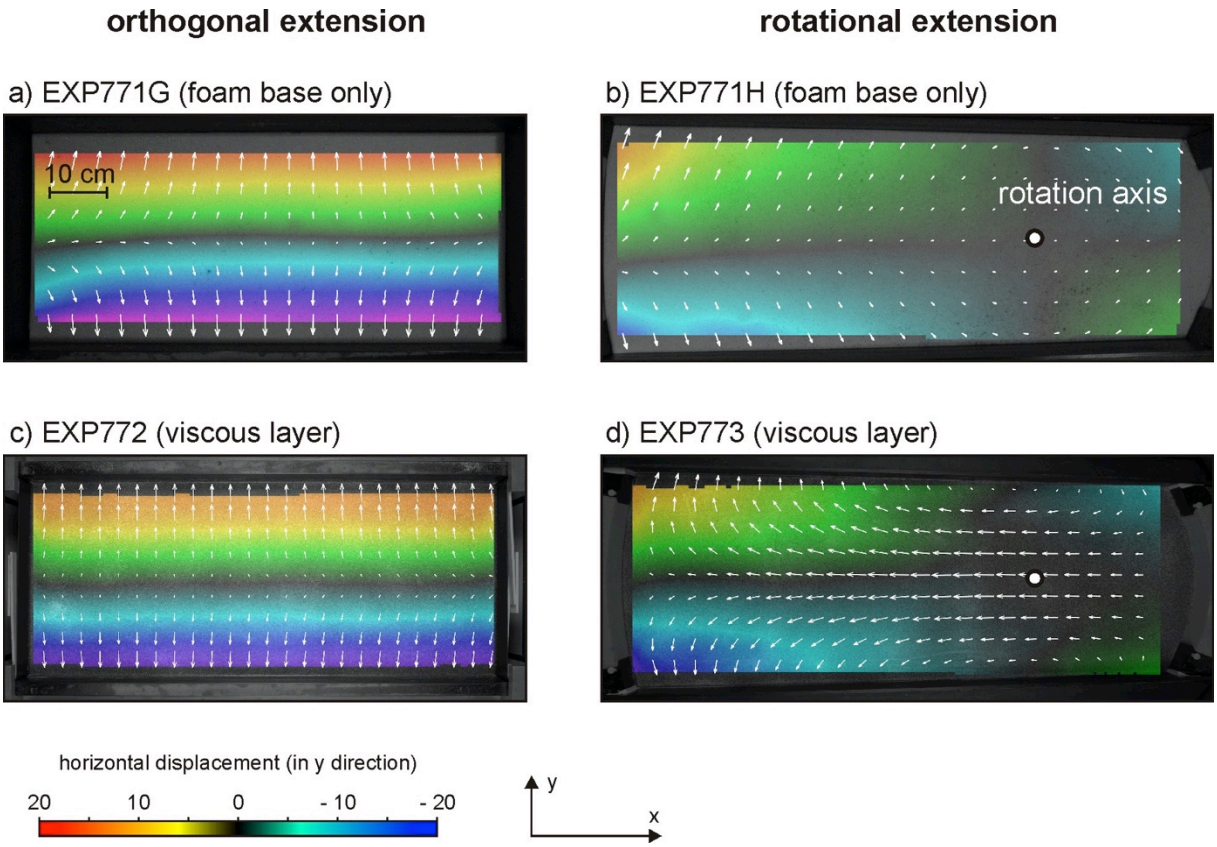

Figure 4: Overview of DIC surface displacement results from Benchmark models. *Color-coded map and vectors of cumulative across-strike (y-) displacement. See movies included in this data set.*

2.1.2. Models with partial seeds

The analogue model series presented in this Data Publication does not only explore the differences between orthogonal and rotational extension, but also the effects of the length of structural weaknesses (or "seeds", see Zwaan et al., 2019) on rift development and propagation (Table 1). A full overview of the final cumulative horizontal displacement derived from DIC analysis is presented in Fig. 5 (see also the movies for a detailed insight in model evolution).

The experimental results show that models without a seed (EXP678 and 679) do not develop any central rift structure. Instead, all externally applied extension is accommodated by boundary effects along the longitudinal sidewalls. On the other hand, adding a seed along the full length (EXP661 and EXP666) leads to concentration of deformation along the axis of the rift. In the case of orthogonal extension (EXP661), a cylindrical rift structure that forms, whereas the rotational extension experiment (EXP666) develops a structural gradient along its center, including contractional features on the opposite side of the rotation axis. Such rotation is also strongly associated with rift propagation and the formation of V-shaped basins (Zwaan et al. 2019). It must however be noted, that even in these full-seed models, about half of the externally applied extension is lost to strain partitioning between the central rift and boundary effects.

When applying partial seeds, a rift structure develops above these seeds, and subsequently propagates laterally towards the part of the model without seed (Fig. 5). The degree of propagation depends on the length of the seed. A ¼ L seed (L = length of the model) leads to limited propagation, whereas seeds longer than ½ L develop full-length rift structures, which are very similar to the 1 L seed results, although the rifts are slightly wider where no seed is present, due to the locally thicker sand layer. In the case of the ¼ L models (EXP681 and EXP682), a combination of both end members develops: where a seed is present, strain is partitioned between the central rift and the model boundaries (similar to the full-seed models) but where no seed is available, deformation is taken up by boundary effects (similar to the models without seed). Between these two domains, a transition occurs where the rift attempts to propagate. This removes deformation from the sidewalls, leading to an along-strike gradient in boundary effects, which itself leads to local block rotation, best visible in EXP681 (since EXP682 itself has rotational boundary conditions that overprint its deformation patterns). These results suggest that also in orthogonal extension settings, rift propagation is also associated with (local) rotational motion.

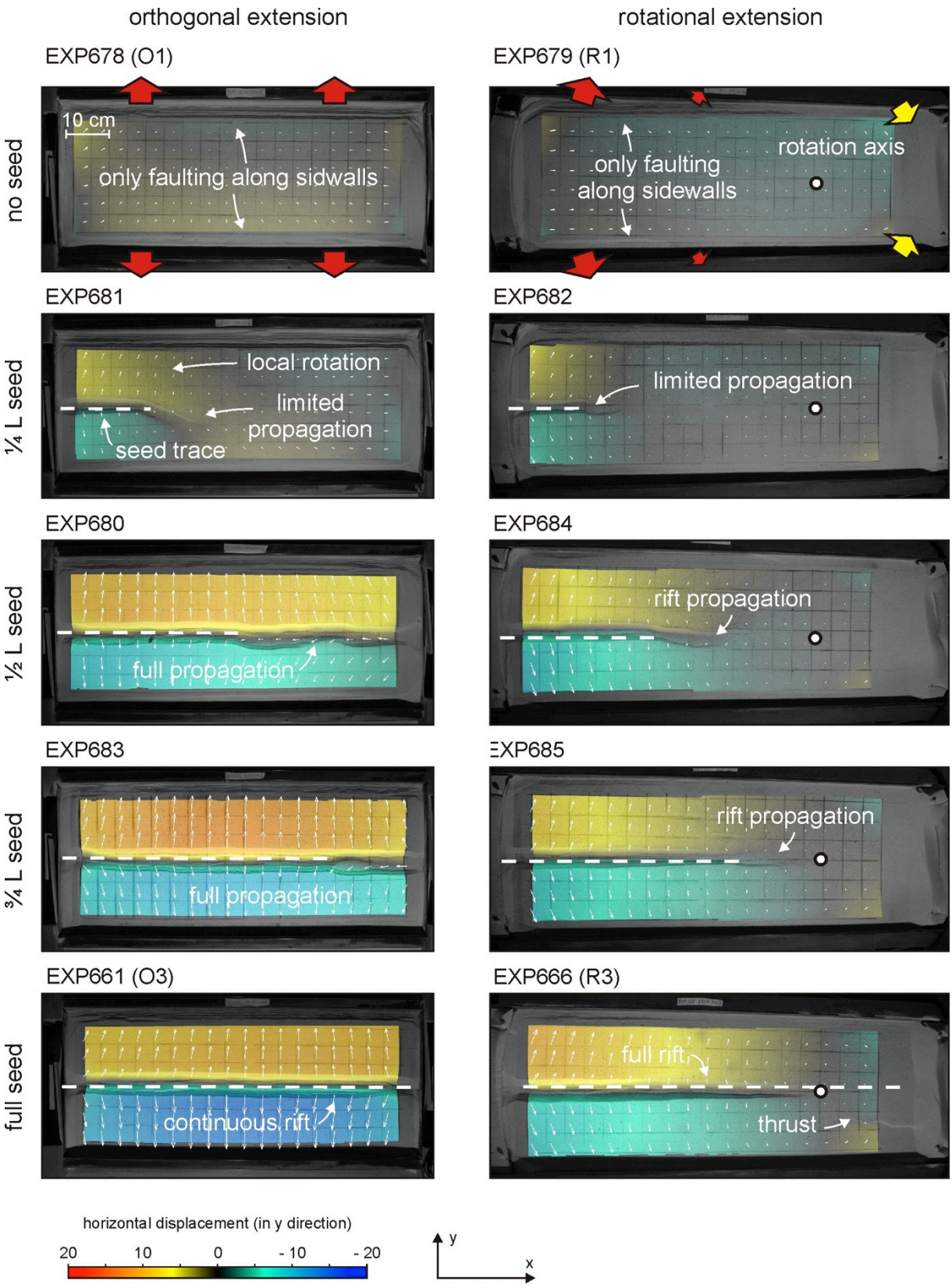

Figure 5: Overview of DIC analysis results in map view. *White arrows indicate total cumulative horizontal displacement, whereas colors display across-strike displacement (i.e. in y-direction) after 40 mm of extension. Dotted lines indicate the seed trace. Circles indicate the location of the rotation axis in rotational extension experiments. 1 L = full model length.*

3. File description

For each of the 10 experiments and four benchmarks we provide:

(i) Movies of surface deformation (avi format)
(ii) Data of cumulative along-strike and across-strike profiles of surface-displacement (prm format)
(iii) Movies of internal deformation (avi format)
(iv) Matlab-script for plotting the profile data
(v) Images of the plotted profile data (bmp format)

An overview of all files of the data set is given in the **List of Files.** For all experiments, movies show cumulative y-displacement of the experimental surface ("*Lab code UB_DIC_cum.avi* "). For the two experiments monitored with the CT-scanner, an additional movie is provided showing the displacement field in the across-strike cross sections of the CT-derived imagery. Profile data and corresponding Matlab-scripts are stored in subfolders ("*Lab code UB_DIC_cum_profiles*"). The name of the basic profile data (e.g. "*EXP661_Cum30_2D-DIC_TS_MP(1x32x32_50ov)_Vy_x360-y-t*.prm") contains information about the DIC parameters (e.g. MP(1x32x32_50ov): interrogation 2D window size: 32x32; 50% overlap, Vy: y-component of displacement vector, x360: x-position of the profile). The profile data file is structured as shown in Table 2.

Table 2: Example of profile data file (EXP661). *For each profile shown in the diagram, the profile position and values of the y-displacement are listed in two columns.*

%position/mm	y-displacement/mm	position/mm	y-displacement/mm	…
298.825989	0.000000	298.825989	0.000000	…
293.782501	0.000000	293.782501	0.000000	…
…	…	…	…	…

4. References

Adam, J., Klinkmüller, M., Schreurs, G. & Wieneke, B. (2013). Quantitative 3D strain analysis in analogue experiments simulating tectonic deformation: Integration of X-ray computed tomography and digital volume correlation techniques. *Journal of Structural Geology*, 55, 127-149, https://doi.org/10.1016/j.jsg.2013.07.011

Adam, J., Urai, J. L., Wieneke, B., Oncken, O., Pfeiffer, K., Kukowski, N., Lohrmann, J., Hoth, S., van der Zee, W & Schmatz, J. (2005). Shear localisation and strain distribution during tectonic faulting – New insights from granular-flow experiments and high-resolution optical image correlation techniques. *Journal of Structural Geology*, 27(2), 283-301, https://doi.org/10.1016/j.jsg.2004.08.008

Zwaan, F., Schreurs, G., Naliboff, J. & Buiter, S. J. H., 2016. Insights into the effects of oblique extension on continental rift interaction from 3D analogue and numerical models. *Tectonophysics*, 693, 239-260, https://doi.org/10.1016/j.tecto.2016.02.036

Zwaan, F., Schreurs, G. & Rosenau, M. (2019). Rift development and propagation under orthogonal versus rotational extension conditions as observed in 4D analogue models. https://doi.org/10.1016/j.jsg.2019.103946